3.4.3 CTSK2d

A. Algorithm Outline

(1) Algorithm Code: CTSK2d

(2) Product Code: SNGI, SNGI_p

(3) PI Name: Dr. Knut Stamnes

(4) Overview of Algorithm

The algorithm presented in this document consists of two parts: the retrieval of sea surface temperatures for an open ocean area, and the retrieval of snow/ice surface temperatures for an ocean area covered by snow/ice. This algorithm can also be applied to snow-covered land, if the snow depth is larger than 5 cm. It works only under clear-sky conditions. Even though the method and the technique used in this algorithm are similar to those used in estimating sea and land surface temperatures, this algorithm has been developed specifically for the polar regions and for the use with GLI measurements. The IST part of this algorithm is the primary surface temperature algorithm since the Arctic surface is covered with snow/ice most of the year. The SST part of this algorithm will be applied to a mixture of snow/ice and water.

Although the thermal emissivity of snow/ice is quite insensitive to surface parameters including density, grain size, thickness, liquid water content, and impurity content (Dozier and Warren, 1982; Warren, 1982), it has an angular and spectral dependency. In this study the MODTRAN radiative transfer model is employed to simulate the radiances measured by the satellite sensor (e.g., GLI) using the directional snow emissivities that are computed with the DISORT radiative transfer model. Since MODTRAN has a 2 cm^{-1} spectral resolution, it is accurate enough for the purpose of this study.

To simulate radiances in GLI and MAS (MODIS Airborne Simulator) thermal channels, daily temperature and humidity profiles are used in the MODTRAN radiative transfer model. Radiosonde ascents over the entire Arctic are taken from the NCEP/NCAR (National Center for Atmospheric Research) Arctic Marine Rawinsonde archive. This data set contains 17,659 reports of ship (marine) rawinsondes (i.e., radiosondes: tracked from the ground by radar to measure variations in wind direction and wind speed with altitude) for the region north of 650. Its record extends from 1976 to 1996. Sounding data from this NCAR Rawinsonde archive cover different atmospheric conditions (such as those caused by regional and seasonal variations).

B. Theoretical Description

(1) Physical and Mathematical Aspects of the Algorithm

The simple approach for atmospheric correction is to measure radiation from a given field of view at two or more window frequencies having different atmospheric absorption. The sea surface temperature can then be estimated as a linear combination of measured brightness temperatures at these frequencies:

$$T_S = a(\theta) + \sum_{i=1}^{n} b_i(\theta) T_i \tag{2.1}$$

where T_S is the measured surface temperature, θ is the satellite scan angle, $a(\theta)$ and $b_i(\theta)$ are scan angle-dependent coefficients, T_i is the measured brightness temperature in each thermal channel i, and n is the total number of channels used. The minimization of errors in the T_S measurements is dependent on the correct choice of the coefficients $a(\theta)$ and $b_i(\theta)$.

There are two ways to determine the coefficients. One approach is to relate satellite observations to surface temperature measurements with a simple regression model. However, for a robust solution a relatively large set of high-quality *in-situ* temperature and satellite data is required. The other approach is the simulation method. A radiative transfer model is used together with a large set of atmospheric profiles to simulate the satellite measurements under a wide range of atmospheric conditions and surface temperatures. The simulated measurements are then used with a set of assigned surface temperature values to derive the coefficients, again by regression analysis.

Instead of computing a different set of coefficients for each scan angle increment, as shown in (2.1), here we use the equation

$$T_S = a + b\,T_{11} + c\,(T_{11}-T_{12}) + d\,[(T_{11}-T_{12})\,(\sec\theta - 1)] \tag{2.2}$$

where T_S is the estimated surface temperature (in K), T_{11} and T_{12} are the brightness temperatures (in K) at 11 μm (GLI channel 35, MAS channel 45) and 12 μm (GLI channel 36, MAS channel 46), respectively, and θ is the sensor scan angle. Coefficients a, b, c, and d are derived from multilinear regression. This approach using two "split-window" infrared channels at approximately 11 μm and 12 μm is commonly employed for SST retrieval (Minnett, 1990; Llewellyn-Jones *et al.,* 1984; Barton, 1985), IST retrieval (Key and Haefliger, 1992; Key *et al.,* 1997), and snow-free LST retrieval (Key *et al.*, 1997; Wan and Dozier, 1996).

(2) Methodology and Logic Flow

For reaching high accuracy the MODTRAN radiative transfer model is employed for simulating the radiances measured by GLI and MAS. In MODTRAN a narrow-band model is used for computing gaseous optical depth from the HITRAN database with wavenumber steps of 1 cm^{-1}. Then the MODTRAN has a spectral resolution of 2 cm^{-1} at FWHM (Full Width at Half-Maximum) with averaged steps of 1 cm^{-1}. Multiple scattering is also included in the radiative transfer model by combining MODTRAN (refer: MODTRAN version 3.5) and DISORT. For the GLI and MAS instruments, since the sensor scan angle lies between 0° and 50°, our simulations are done for viewing angles in the range of 0°-50° with increments of 5°. The built-in standard subarctic winter and summer atmospheric profiles including trace gases and the background aerosol model in MODTRAN are used in our simulations. Blanchet and List (1983) showed that the volume extinction coefficient of Arctic haze is generally of the same order of magnitude as troposphere aerosols. Thus we use troposphere background aerosol instead of Arctic haze. The calculations of retrieval coefficients in Eq. (2.2) using both GLI and MAS channels are presented in this document for testing and validating the algorithm. The sensor response functions both for GLI channels 35 and 36 and for MAS channels 45 and 46 are used to compute radiances at the top of the atmosphere, and the radiances are then converted to brightness temperature by use of the Planck function.

For IST retrieval, the surface is assumed to be snow/ice-covered. Directional surface emissivities for snow are calculated based on an extended version of the DISORT radiative transfer model appropriate for the coupled atmosphere-surface system. This algorithm allows us to study the bidirectional reflectance and directional emissivity for a surface covered with different types of snow and sea ice. Coefficients *a, b, c*, and *d* in Eq. (2.2) for IST retrieval are calculated within the following three temperature ranges: (i) $T_{11} < 240\ K$; (ii) $240\ K < T_{11} < 260\ K$; and (iii) $260\ K < T_{11} < 271.4\ K$.

We now assume that the freezing point of sea water is 271.4 *K* based on the average freezing point of empirical and reported values (Bialek, 1966; Massom and Comiso, 1994; Yu and Rothrock, 1996; Riggs *et al.,* 1997). For temperatures above the melting point, a mixture of snow/ice and meltponds occurs. In such cases the code for open ocean SST retrieval will be applied. An equation similar to Eq. (2.2) will be used, but the surface emissivities are assumed to be an area-weighted sum of snow and water emissivities. For the surface temperature retrieval of an area with a mixture of snow/ice and meltponds, only two situations are studied here, i.e., (i) for $T_{11} < 275\ K$, the weights are 0.8 for snow and 0.2 for water, respectively; and (ii) for $T_{11} > 275\ K$, the weights are 0.2 for snow and 0.8 for water. Obviously, the approximation of dividing all the cases with the presence of melt ponds into just two categories will lead to an uncertainty in the estimated surface temperature.

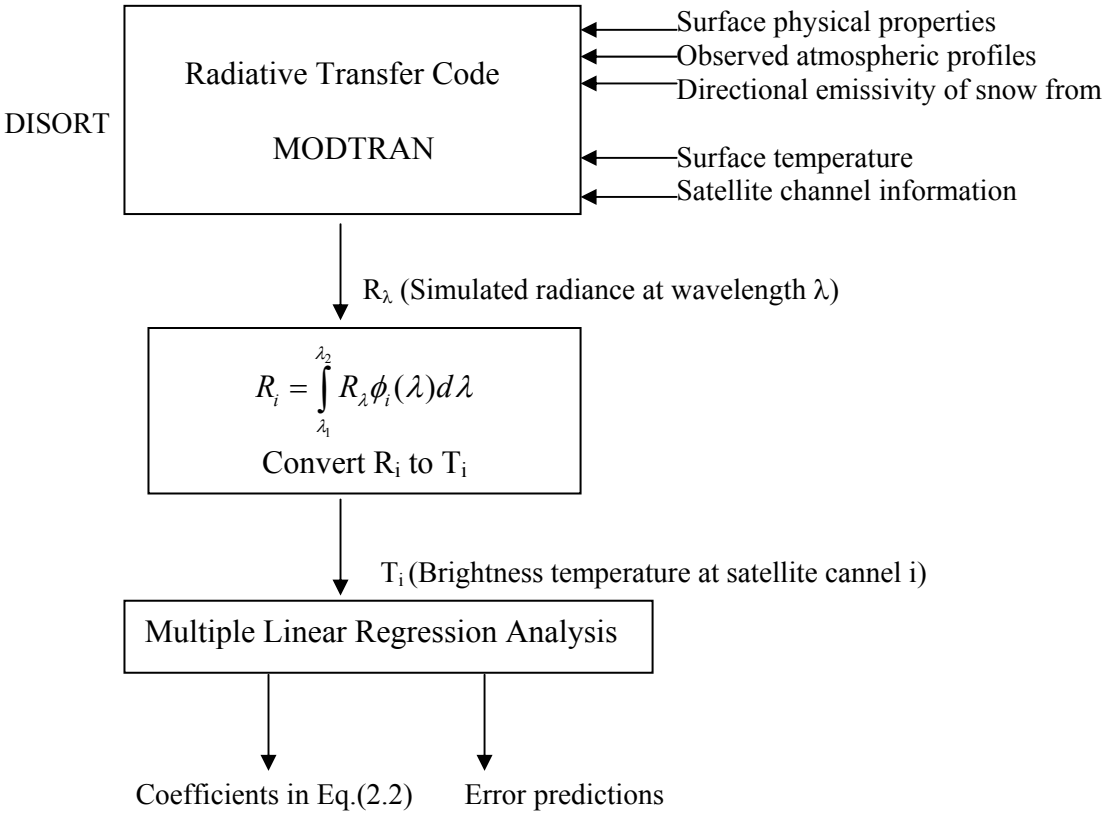

Fig.2.1 Flow chart for the numerical simulations of satellite measurements.

The procedure to determine the coefficients in Eq. (2.2) is summarized as follows (see Fig. 2.1). The surface physical properties, observed atmospheric profiles, sensor response function, and snow directional emissivities data calculated using the extended version of DISORT are input into MODTRAN to simulate radiances at MAS or GLI channels for a wide range of atmospheric conditions. In these simulations, the temperature of the first layer just above the surface is taken as the surface temperature. The simulated radiances are integrated with the sensor response functions for the MAS or GLI channels:

$$R_i = \int_{\lambda_1}^{\lambda_2} R(\lambda)\phi_i(\lambda)d\lambda \tag{2.3}$$

where R_i is the simulated radiance, and φ_i is the sensor response function for channel i. Then, the integrated, simulated radiances R_i are converted to brightness temperatures T_i. A least-squares multilinear regression is used to determine the coefficients in Eq. (2.2). The coefficients in Eq. (2.2) for the IST and SST algorithms are presented in Tables 2.1 and 2.2, respectively. The correlation coefficients between estimated and actual surface temperature as well as the RMSE (root-mean-square errors) are also given in Tables 2.1 and 2.2.

Table 2.1a The coefficients in Eq. (2.2) for IST algorithm using MAS data

Temperature range (*K*)	a	b	c	d	Correlation coefficient	RMS
< 240	-1.157655	1.005439	1.535782	2.239843	0.9997583	0.054294
240 - 260	-1.587060	1.007282	1.500379	1.595407	0.9999706	0.045863
260-271.4	-2.480842	1.010931	1.447117	1.087111	0.9997824	0.067924

Table 2.1b The coefficients in Eq. (2.2) for IST algorithm using GLI data

Temperature range (*K*)	a	b	c	d	Correlation coefficient	RMS
< 240	-0.504486	1.00195	1.29798	-0.701453	0.999874	0.039571
240 - 260	-0.688521	1.00274	0.912788	0.970363	0.999981	0.036509
260-271.4	-1.238140	1.00524	0.775538	0.566395	0.999885	0.043058

Table 2.2a The coefficients in Eq. (2.2) for SST algorithm using MAS data

Temperature range (*K*)	a	b	c	d	Correlation coefficient	RMS
271.4 - 275	-5.607100	1.022034	1.725736	1.250851	0.9980459	0.063624
> 275	-2.740712	1.011390	1.993035	1.331676	0.9997357	0.063551

Table 2.2b The coefficients in Eq. (2.2) for SST algorithm using GLI data

Temperature range (*K*)	a	b	c	d	Correlation coefficient	RMS
271.4 - 275	-2.09631	1.00823	0.885022	0.477340	0.998565	0.045994
> 275	-3.79538	1.01408	1.09925	0.424474	0.999717	0.056158

In order to develop an algorithm using the split-window technique specifically for polar regions, atmospheric profiles from the NCEP/NCAR Arctic Marine Rawinsonde Archive are used for simulating the sensor-measured radiances. More than 4000 radiosonde profiles are used for the surface temperature (both SST and IST) algorithm development. The data set from the NCEP/NCAR Arctic Marine Rawinsonde Archive covers a large range of atmospheric conditions including different seasons and different locations across the Arctic.

C. **Practical Considerations**

(1) Programming Requirements

The following table shows information about the expected software generated from this algorithm:

Table 3.1 Program Requirements

Program Memory	400 KBytes
Program Size	100 KBytes
Required Channels	35, 36
Necessary/Ancillary Data	

Expected Disk Volume	
Special Programs or Subroutines	
Look-up tables	none

(2) Calibration and Validation

Based on Tables 2.1 and 2.2, we apply the surface temperature retrieval algorithm discussed above to estimate the surface temperature using GLI-observed data. This algorithm can only be applied to cloud-free pixels over the snow. Before this surface temperature retrieval algorithm is executed, the cloudy/clear and snow/sea-ice discriminators (cf. ATBD for CTSK1a and CTSK1b submitted to NASDA by Knut Stamnes, PI of the contract A2GSF004 for GLI program) will be applied for distinguishing cloudy-free snow pixels from cloudy pixels and other surface pixels. Then, for identified cloud-free pixels, the surface temperatures are estimated based on Eq. (2.2) and the coefficients given in Tables 2.1b and 2.2b according to the brightness temperature in GLI channel 35.

In order to assess the accuracy of this surface temperature retrieval algorithm, we use the MODTRAN radiative transfer model with the standard subarctic winter atmospheric profile to simulate the brightness temperature at both MAS channels 45 and 46, and GLI channels 35 and 36 for the viewing angles of 0°, 10°, 20°, 30°, and 40°, respectively. Due to the lack of surface temperature data and the difficulty of defining appropriate boundary layer conditions for all surface types and locations, the temperature of the first layer of the profile, 257.2 *K*, is taken as the surface temperature (Key *et al*., 1997). Of course, this assumption will lead to some uncertainties, since the difference between surface temperature and air temperature of the first layer can be significant for some situations. Then, the surface temperature retrieval algorithm is executed with brightness temperatures BT_{35} and BT_{36} (or BT_{35} and BT_{36} for MAS data) obtained from forward calculations using the MODTRAN radiative transfer model for different viewing angles. The estimated surface temperature T_S is obtained from Eq. (2.2), and listed in Table 3.2. The differences (ΔT) between the given surface temperature (T_G) of the forward simulation and the estimated surface temperature (T_S) of the inverse retrieval are also shown in Table 3.2. From Table 3.2, the accuracy of the algorithm is better than 0.12 *K*.

Table 3.2a. The retrieved surface temperature for MAS channels (T_G = 257.2 *K*).

View angle	0°	10°	20°	30°	40°
BT_{45}	256.6921	256.6884	256.6777	256.6547	256.6187
BT_{46}	256.5797	256.5770	256.5684	256.5522	256.5252
T_S	257.1429	257.1404	257.1321	257.1157	257.0834
$\Delta T = T_G - T_S$	0.0571	0.0596	0.0679	0.0843	0.1166

Table 3.2b. The retrieved surface temperature for GLI channels (T_G = 257.2 *K*).

View angle	0°	10°	20°	30°	40°

BT_{35}	256.90	256.90	256.90	256.88	256.83
BT_{36}	256.65	256.62	256.62	256.60	256.55
Ts	257.1436	257.1752	257.1884	257.1929	257.1838
$\Delta T = T_G - T_S$	0.0564	0.0248	0.0116	0.0071	0.0162

Fig.3.1 shows the retrieved surface temperature distribution based on the GLI observation made on April 14 (Fig. 3.1a), and April 26 (Fig. 3.1b), 2003 over Barrow, Alaska. White color area is for cloud pixels. These retrieved surface temperatures look very reasonable. We also compared these data with the simultaueous field measured data at the Barrow site (71°18′00″N, 156°35′00″W) (See Table3.3). We use the average temperature at a 5×5 pixel box around the field site to indicate the retrieval data. From the results, we will find IST retrieval shows a good match, but SST retrieval is underestimated.

Table 3.3 Comparison with match-up data at Barrow site

GLI image	Pixel/line in image	Field measured surface temperature	Retrieved 5×5 box average temperature
2003041453	1156/580	- 7°C (266K)	266.215K
2003041457	482/279	-4.5°C (268.5K)	267.321K
2003042653	1156/580	0.5°C (273.5K)	269.615K
2003042657	482/279	3.0°C (276K)	270.917K

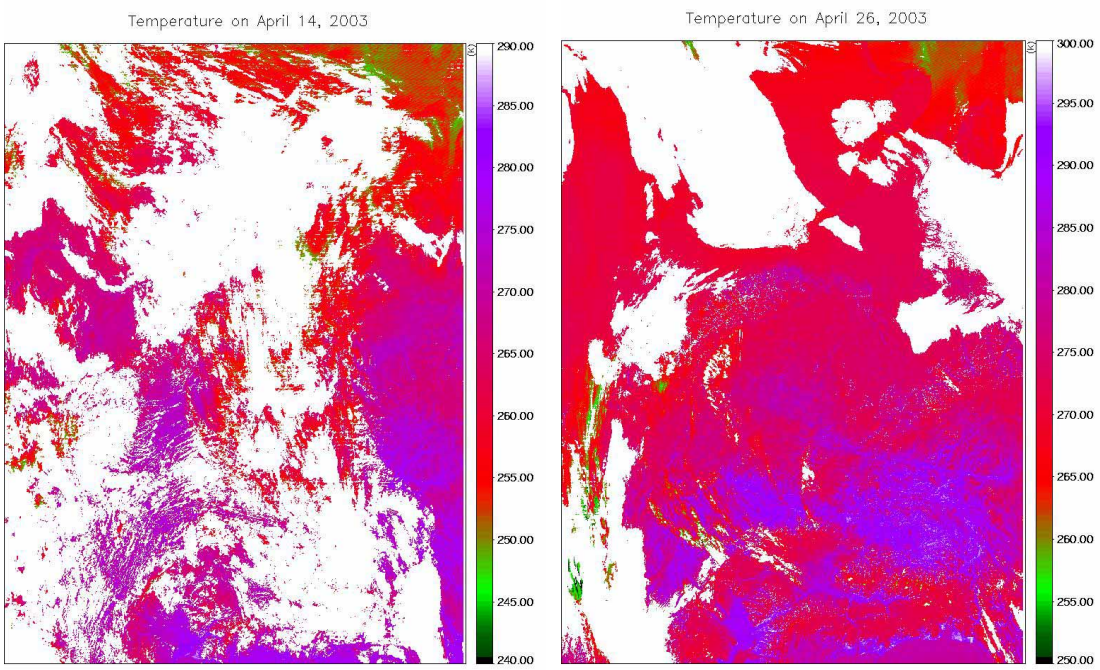

Fig. 3.1 The retrieved surface temperature from the GLI data over Barrow of Alaska on (a) April 14, 2003 and (b) April 26, 2003.

(3) Quality Control and Diagnostic Information

(4) Exception Handling

(5) Constraints, Limitations, Assumptions

At present time, this algorithm is implemented for the analysis of clear-sky snow pixels over the polar regions and mid-latitude regions (between 20° and 60° in latitude).

(6) Publications and Papers

D. References

Barton, I.J., 1985: Transmission model and ground-truth investigation of satellite-derived sea surface temperatures, *J. Clim. Appl. Meteorol*., **24**, 508-516.

Bialek, E.L., 1966: Handbook of Oceanographic Tables. Special Publication, SP-68, U.S. Naval Oceanographic Office, Washington D.C..

Blanchet, J. and R. List, 1983: Estimation of optical properties of arctic haze using a numerical model. *Atmos. Ocean*., **21**, 444-465.

Dozier, J. and S.G. Warren, 1982: Effect of viewing angle on the infrared brightness temperature of snow. *Water Resour. Res*., **18**, 1424-1434.

Key, J., and M. Haefliger, 1992: Arctic ice surface temperature retrieval from AVHRR thermal channels. *J. Geophys. Res*., **97**, 5885-5893.

Key, J.R., J.B. Collins, C. Fowler, and R.S. Stone, 1997: High-latitude surface temperature estimates from thermal satellite data. *Remote Sens. Environ*., **67**, 302-309.

Llewellyn-Jones, D.T., P.J. Minnett, R.W. Saunders, and A.M. Zavody, 1984: Satellite multichannel infrared measurements of sea surface temperature of the northeast Atlantic Ocean using AVHRR/2. *Q. J. R. Meteorol. Soc*., **110**, 613-631.

Massom, R. and J.C. Comiso, 1994: The classification of Arctic sea-ice types and the determination of surface temperature using advanced very high resolution radiometer data. *J. Geophys. Res*., **99**, 5201-5218.

McClain, E.P., W.G. Pichel, and C.C. Walton, 1985: Comparative performance of AVHRR-based multichannel sea surface temperature. *J. Geophys. Res*., **90**, 11587-11601.

Minnett, P.J., 1990: The regional optimization of infrared measurements of sea surface temperature from space. *J. Geophys. Res*., **95**, 13497-13510.

Price, J.C., 1983: Estimating surface temperature from satellite thermal infrared data -- a simple formulation for the atmospheric effect. *Remote Sens. of Environ*., **13**, 353-361.

Riggs, G.A., D.K. Hall, and S.A. Ackerman, 1997: Sea ice detection with the Moderate Resolution Imaging Spectroradiometer Airborne Simulator (MAS). *Remote Sens. of Environ.*, in press.

Wan, Z. and J. Dozier, 1996: A generalized split-window algorithm for retrieving land-surface temperature from space. *IEEE Trans. Geosci. Remote Sens*., 34, 892-905.

Warren, S.G., 1982: Optical properties of snow, *Rev. Geophy. Space Phys*., **20**, 67-89.

Yu, Y. and D.A. Rothrock, 1996: Thin ice thickness from satellite thermal imagery. *J. Geophys. Res*., **101**, 25753-25766.